On the Capacity of Decode-and-Forward FSO System With Single- and Dual-Hop RF Link

Essam Saleh Altubaishi, *Member, IEEE*, and Wagdy Ameen Alathwary, *Graduate Student Member, IEEE*

***Abstract*—In this study, we consider two dual-hop FSO systems with decode-and-forward protocol. The FSO system is assumed to be equipped with RF link used as a backup in case the FSO link experiences strong atmospheric turbulence or pointing errors. The two system models differ by the setup of the RF link. A single-hop RF backup link is used for the first system model, whereas a dual-hop RF backup link is used for the second system model. We assume that the FSO system uses intensity modulation with direct detection and the channel is modeled by gamma-gamma distribution, and the RF channel is modeled by Nakagami-m distribution. The performance of both system models is studied in terms of ergodic capacity where new expressions are derived and compared with the results of Monte Carlo simulations. The results indicate the improvement of the spectral efficiency compared to the conventional dual-hop FSO system.**

***Index Terms*—Free space optics, hybrid system, strong atmospheric turbulence, average capacity.**

I. Introduction

FREE space optical (FSO) communication has gained significant attention due to its capability to support high capacity which becomes a good candidate for the future high-speed wireless networks. The major effects that may degrade its performance are the atmospheric turbulence, pointing errors, and weather attenuation [1], [2]. One way to tackle these effects is to use mixed or hybrid FSO-radio frequency (RF) system supported by relaying techniques.

In [3], the dual-hop FSO system with decode-and-forward (DF) was studied using intensity modulation/direct detection (IM/DD). The effect of pointing errors on the capacity of the system under different turbulence conditions was investigated. Same system model of [3] was adopted in [4] but with amplify-and-forward (AF) protocol where the performance was analyzed in terms of symbol error rate (SER) and capacity. Later, the work of [5] derived unified expressions for the average bit error rate (BER) and outage probability of mixed RF–FSO system in which a generalised distribution for RF link was considered. The authors in [6] further investigated the system by assuming co-channel interference in the RF link. In [7], outage probability of mixed RF-FSO system with multi-diversity and combining was derived where the fading of RF links and the atmospheric turbulence of FSO links were assumed to follow Rayleigh and gamma-gamma distributions, respectively. Similar distributions were used in [8] to study the ergodic capacity of the mixed RF-FSO system. The authors in [9] considered mixed FSO-RF system with Málaga fading channel for FSO link and Rayleigh fading channel for RF link. The outage probability and BER were studied under the effect of pointing error as well. Moreover, the work in [10] investigated the performance of the system assuming that FSO link follows double generalized gamma distribution and RF link follows extended generalized-K distribution. In [11], the performance of the mixed system over gamma-gamma/α-$\mathcal{F}$ distributions is studied where expressions for the ergodic capacity, outage probability, and average BER are derived. In the above-mentioned mixed RF-FSO systems, the capacity of the system is limited by the RF link capacity.

To resolve this limitation, a hybrid system has been introduced. The hybrid system exploits the differences in the properties of FSO and RF channels to create a complementary system. In this system, the FSO channel is more susceptible to severe turbulence or dense fog, while the RF channel is more affected by heavy rain. A single-hop hybrid system was proposed in [12], where FSO link starts the transmission as long as its quality is above a certain level, otherwise, the system switches to RF link. In [13], the authors also investigated the single-hop hybrid system but under gamma-gamma fading and point errors. The work of [14] added a maximal ratio combiner at the receiver when the RF link is activated. Furthermore, a single-hop hybrid system was investigated in [15] and [16] with different combining schemes. In [17], a dual-hop switching-based hybrid system with combining technique at destination was proposed and investigated, where expressions for the outage probability and average SER were derived. In [18], we proposed a dual-hop FSO system with direct RF backup link using amplify-and-forward protocol and under log-normal atmospheric turbulence model for FSO link and Rayleigh fading model for RF link. The work in [19] considered a dual-hop hybrid FSO/RF system with direct transmission in which a selective combining technique is used at destination. The work derived an expression for the average SER using infinite series form.

In this work, we aim to investigate the capacity performance of two system models of hybrid FSO/RF system. Unlike [12], [13], [14], [15], [16], both of our systems consist of a dual-hop

Manuscript received 10 September 2023; revised 6 November 2023; accepted 5 December 2023. Date of publication 14 December 2023; date of current version 29 December 2023. This work was supproted by the Researchers Supporting Program, King Saud University, Riyadh, Saudi Arabia, under Grant RSPD2023R842. *(Corresponding author: Essam Saleh Altubaishi.)*

The authors are with the Department of Electrical Engineering, King Saud University, Riyadh 11421, Saudi Arabia (e-mail: etubashi@ksu.edu.sa; walathwary@ksu.edu.sa).

Digital Object Identifier 10.1109/JPHOT.2023.3341080

FSO link. In contrast to [18], our systems utilize the DF protocol for signal forwarding, with assuming that the FSO link experiences gamma-gamma turbulence and pointing errors, where the gamma-gamma model is commonly used in FSO communication systems due to its ability to accurately capture the effects of atmospheric turbulence on the optical signal and provides a good representation of scintillation and fading phenomena. Distinct from [17], [19], our systems do not require a combining technique at the receiver. The first system model has a single-hop RF backup link, while the second system model contains dual-hop RF backup link. Nakagami-m fading is assumed for the RF link which covers different channel fading scenarios like Rayleigh and Rician by varying its parameter m. This choice enables the Nakagami-m model to accurately represent the RF channel in our system, which comprises two different RF setups. Exact expressions for the ergodic capacity are derived for both systems after obtaining the required cumulative distribution functions (CDFs) and probability density functions (PDFs). We investigate the performance of the two system models and compare it with Monte Carlo simulations.

The rest of the paper is structured as follows. The two system models are presented in Section II in addition to the end-to-end signal-to-noise ratio (SNR) statistical characteristics. In Section III, exact expressions for the ergodic capacity are derived. Results are given in Section IV. Finally, Section V concludes the paper.

II. System Overview

In this work, we consider two system models; dual-hop FSO system with single-hop RF backup link and dual-hop FSO system with dual-hop RF backup link. The relay node uses DF protocol for both FSO and RF links. A feedback channel is used to switch from FSO link to backup RF link if FSO link can not support the target quality. The FSO link uses intensity modulation/direct detection (IM/DD) technique with phase-shift-keying (PSK) modulation scheme [12]. The atmospheric turbulence of the FSO link is modeled by gamma-gamma distribution, then the probability density function (PDF) of the instantaneous signal-to-noise ratio (SNR) γ_i^{FSO} of the ith hop with pointing errors is given by

$$f_{\gamma_i^{FSO}}(\gamma) = \frac{\phi_i^2}{2\,\Gamma(\alpha_i)\,\Gamma(\beta_i)\,\gamma} \times \mathrm{G}_{1,3}^{3,0}\left[\alpha_i\,\beta_i\,\xi_i\left(\frac{\gamma}{\bar{\gamma}_i^{FSO}}\right)^{\frac{1}{2}}\middle|\begin{matrix}\phi_i^2+1\\ \phi_i^2,\alpha_i,\beta_i\end{matrix}\right], \quad (1)$$

where $\Gamma(\cdot)$ is the gamma function, $\mathrm{G}_{\cdot,\cdot}^{\cdot,\cdot}(\cdot)$ is the Meijer G function, $\gamma_i^{FSO} = (P_{FSO,i}^2\,{\eta_i}^2\,h_{FSO,i}^2)/\sigma_{n,FSO}^2$, $P_{FSO,i}$ is the FSO transmitted power, η_i is the receiver responsivity, $h_{FSO,i}$ is FSO channel fading, and $\bar{\gamma}_i^{FSO} = (P_{FSO,i}^2\,{\eta_i}^2\,A_{0,i}^2\,\xi_i^2\,{h_{FSO,i}^l}^2)/\sigma_{n,FSO}^2$ is the average SNR, $A_{0,i}$ is a parameters related to pointing errors, $\xi_i = \phi_i^2/(\phi_i^2+1)$, $\phi_i = w_{L_{eq},i}/2\,\sigma_{s,i}$, where $\sigma_{s,i}$ is the standard deviation of the jitter at the receiver, α_i and β_i are the effective numbers of small- and large-scale turbulence parameters, respectively, and $h_{FSO,i}^l$ is the atmospheric attenuation which is given by [20]

$$h_{FSO,i}^l = \frac{\pi R_{o,i}^2}{(\theta_i L_i)^2}\exp\left(-\sigma_i L_i\right), \quad (2)$$

where $R_{o,i}$ is the radius of receiver aperture, θ_i is the divergence angle, σ_i is the atenuation factor and L_i is the hop length. The cumulative distribution function (CDF) of γ_i^{FSO} is found by integrating (1) in terms of γ and using [21] which can be written as

$$F_{\gamma_i^{FSO}}(\gamma) = \frac{2^{\alpha_i+\beta_i-3}\,\phi_i^2}{\pi\,\Gamma(\alpha_i)\,\Gamma(\beta_i)}\mathrm{G}_{3,7}^{6,1}\left[\left(\frac{\alpha_i\,\beta_i\,\xi_i}{4}\right)^2\frac{\gamma}{\bar{\gamma}_i^{FSO}}\middle|\begin{matrix}1,\frac{\phi_i^2+1}{2},\frac{\phi_i^2+2}{2}\\ \frac{\phi_i^2}{2},\frac{\phi_i^2+1}{2},\frac{\alpha_i}{2},\frac{\alpha_i+1}{2},\frac{\beta_i}{2},\frac{\beta_i+1}{2},0\end{matrix}\right]. \quad (3)$$

The instantaneous SNR of the DF dual-hop link is given by

$$\gamma = \min\left(\gamma_1,\gamma_2\right). \quad (4)$$

Then the CDF of the SNR for the FSO link can be obtained as

$$F_{\gamma^{FSO}}(\gamma) = F_{\gamma_1^{FSO}}(\gamma) + F_{\gamma_2^{FSO}}(\gamma) - F_{\gamma_1^{FSO}}(\gamma)\,F_{\gamma_2^{FSO}}(\gamma) \quad (5)$$

Using (3) in (5), closed-from expression for $F_{\gamma^{FSO}}(\gamma)$ can be obtained. Differentiating (5) with respect to γ, then using (1) and (3), $f_{\gamma^{FSO}}(\gamma)$ is given as

$$\begin{aligned}
&f_{\gamma^{FSO}}(\gamma)\\
&= f_{\gamma_1^{FSO}}(\gamma) + f_{\gamma_2^{FSO}}(\gamma) - f_{\gamma_1^{FSO}}(\gamma)F_{\gamma_2^{FSO}}(\gamma)\\
&\quad - F_{\gamma_1^{FSO}}(\gamma)f_{\gamma_2^{FSO}}(\gamma)\\
&= \frac{\phi_1^2}{2\Gamma(\alpha_1)\Gamma(\beta_1)\gamma}\mathrm{G}_{1,3}^{3,0}\left[\alpha_1\beta_1\xi_1\left(\frac{\gamma}{\bar{\gamma}_1^{FSO}}\right)^{\frac{1}{2}}\middle|\begin{matrix}\phi_1^2+1\\ \phi_1^2,\alpha_1,\beta_1\end{matrix}\right]\\
&\quad + \frac{\phi_2^2}{2\Gamma(\alpha_2)\Gamma(\beta_2)\gamma}\mathrm{G}_{1,3}^{3,0}\left[\alpha_2\beta_2\xi_2\left(\frac{\gamma}{\bar{\gamma}_2^{FSO}}\right)^{\frac{1}{2}}\middle|\begin{matrix}\phi_2^2+1\\ \phi_2^2,\alpha_2,\beta_2\end{matrix}\right]\\
&\quad - \frac{2^{\alpha_2+\beta_2-4}\phi_2^2}{\pi\Gamma(\alpha_2)\Gamma(\beta_2)}\mathrm{G}_{3,7}^{6,1}\left[\left(\frac{\alpha_2\beta_2\xi_2}{4}\right)^2\frac{\gamma}{\bar{\gamma}_2^{FSO}}\middle|\begin{matrix}\varepsilon_3\\ \varepsilon_4\end{matrix}\right]\\
&\quad \times \frac{\phi_1^2}{\Gamma(\alpha_1)\Gamma(\beta_1)\gamma}\mathrm{G}_{1,3}^{3,0}\left[\alpha_1\beta_1\xi_1\left(\frac{\gamma}{\bar{\gamma}_1^{FSO}}\right)^{\frac{1}{2}}\middle|\begin{matrix}\phi_1^2+1\\ \phi_1^2,\alpha_1,\beta_1\end{matrix}\right]\\
&\quad - \frac{2^{\alpha_1+\beta_1-4}\phi_1^2}{\pi\Gamma(\alpha_1)\Gamma(\beta_1)}\mathrm{G}_{3,7}^{6,1}\left[\left(\frac{\alpha_1\beta_1\xi_1}{4}\right)^2\frac{\gamma}{\bar{\gamma}_1^{FSO}}\middle|\begin{matrix}\varepsilon_1\\ \varepsilon_2\end{matrix}\right]\\
&\quad \times \frac{\phi_2^2}{\Gamma(\alpha_2)\Gamma(\beta_2)\gamma}\mathrm{G}_{1,3}^{3,0}\left[\alpha_2\beta_2\xi_2\left(\frac{\gamma}{\bar{\gamma}_2^{FSO}}\right)^{\frac{1}{2}}\middle|\begin{matrix}\phi_2^2+1\\ \phi_2^2,\alpha_2,\beta_2\end{matrix}\right],
\end{aligned} \quad (6)$$

where $\varepsilon_1 = 1,\frac{\phi_1^2+1}{2},\frac{\phi_1^2+2}{2},$ $\varepsilon_2 = \frac{\phi_1^2}{2},\frac{\phi_1^2+1}{2},\frac{\alpha_1}{2},\frac{\alpha_1+1}{2},\frac{\beta_1}{2},\frac{\beta_1+1}{2},0,$ $\varepsilon_3 = 1,\frac{\phi_2^2+1}{2},\frac{\phi_2^2+2}{2},$ and $\varepsilon_4 = \frac{\phi_2^2}{2},\frac{\phi_2^2+1}{2},\frac{\alpha_2}{2},\frac{\alpha_2+1}{2},\frac{\beta_2}{2},\frac{\beta_2+1}{2},0.$

For RF link, since Nakagami-m distribution is considered, the PDF of the instantaneous SNR of a given hop is written as

$$f_{\gamma_i^{RF}}(\gamma) = \left(\frac{m_i}{\bar{\gamma}_i^{RF}}\right)^{m_i} \frac{\gamma^{m_i-1}}{\Gamma(m_i)} e^{\frac{m_i\gamma}{\bar{\gamma}_i^{RF}}}, \tag{7}$$

where m_i is the fading parameter ($m_i \geq \frac{1}{2}$), $\gamma_i^{RF} = \bar{\gamma}_i^{RF} h_{RF,i}^2$, $h_{RF,i}$ is the RF channel fading, $\bar{\gamma}_i^{RF} = P_{RF,i} h_{RF,i}^l / \sigma_{n,RF}^2$ is the average SNR, $P_{RF,i}$ is the RF transmitted power, and $h_{RF,i}^l$ is the path loss of the RF link [22]. The PDF can be given in terms of Meijer-G function as

$$f_{\gamma_i^{RF}}(\gamma) = \left(\frac{m_i}{\bar{\gamma}_i^{RF}}\right)^{m_i} \frac{\gamma^{m_i-1}}{\Gamma(m_i)} \mathrm{G}_{0,1}^{1,0}\left[\frac{m_i\gamma}{\bar{\gamma}_i^{RF}}\middle|\begin{matrix}-\\0\end{matrix}\right]. \tag{8}$$

Similarly, the CDF of γ_i^{RF} can be obtained by integrating (8) with respect to γ and using [21] as

$$F_{\gamma_i^{RF}}(\gamma) = \frac{1}{\Gamma(m_i)} \mathrm{G}_{1,2}^{1,1}\left[\frac{m_i\gamma}{\bar{\gamma}_i^{RF}}\middle|\begin{matrix}1\\m_i,0\end{matrix}\right]. \tag{9}$$

In hybrid FSO/RF system with single-hop RF link, we define the CDF and PDF of the SNR as $F_{\gamma_{single}^{RF}}(\gamma) = F_{\gamma_i^{RF}}(\gamma)$, and $f_{\gamma_{single}^{RF}}(\gamma) = f_{\gamma_i^{RF}}(\gamma)$, respectively, where $i = 1$.

In hybrid FSO/RF system with dual-hop RF link ($i = 1, 2$), the CDF of the SNR of the dual-hop RF link is written as

$$F_{\gamma_{dual}^{RF}}(\gamma) = F_{\gamma_1^{RF}}(\gamma) + F_{\gamma_2^{RF}}(\gamma) - F_{\gamma_1^{RF}}(\gamma)\, F_{\gamma_2^{RF}}(\gamma). \tag{10}$$

Using (9) in (10), $F_{\gamma_{dual}^{RF}}(\gamma)$ can be obtained. Similar to the PDF of FSO link, differentiating $F_{\gamma_{dual}^{RF}}(\gamma)$ with respect to γ and using (8) and (9), we get the PDF of SNR of dual-hop RF link as

$$\begin{aligned} f_{\gamma_{dual}^{RF}}(\gamma) &= f_{\gamma_1^{RF}}(\gamma) + f_{\gamma_2^{RF}}(\gamma) - f_{\gamma_1^{RF}}(\gamma) F_{\gamma_2^{RF}}(\gamma) \\ &\quad - F_{\gamma_1^{RF}}(\gamma) f_{\gamma_2^{RF}}(\gamma) \\ &= \left(\frac{m_1}{\bar{\gamma}_1^{RF}}\right)^{m_1} \frac{\gamma^{m_1-1}}{\Gamma(m_1)} \mathrm{G}_{0,1}^{1,0}\left[\frac{m_1\gamma}{\bar{\gamma}_1^{RF}}\middle|\begin{matrix}-\\0\end{matrix}\right] \\ &\quad + \left(\frac{m_2}{\bar{\gamma}_2^{RF}}\right)^{m_2} \frac{\gamma^{m_2-1}}{\Gamma(m_2)} \mathrm{G}_{0,1}^{1,0}\left[\frac{m_2\gamma}{\bar{\gamma}_2^{RF}}\middle|\begin{matrix}-\\0\end{matrix}\right] \\ &\quad - \left(\frac{m_1}{\bar{\gamma}_1^{RF}}\right)^{m_1} \frac{\gamma^{m_1-1}}{\Gamma(m_1)} \mathrm{G}_{0,1}^{1,0}\left[\frac{m_1\gamma}{\bar{\gamma}_1^{RF}}\middle|\begin{matrix}-\\0\end{matrix}\right] \\ &\quad \times \frac{1}{\Gamma(m_2)} \mathrm{G}_{1,2}^{1,1}\left[\frac{m_2\gamma}{\bar{\gamma}_2^{RF}}\middle|\begin{matrix}1\\m_2,0\end{matrix}\right] \\ &\quad - \left(\frac{m_2}{\bar{\gamma}_2^{RF}}\right)^{m_2} \frac{\gamma^{m_2-1}}{\Gamma(m_2)} \mathrm{G}_{0,1}^{1,0}\left[\frac{m_2\gamma}{\bar{\gamma}_2^{RF}}\middle|\begin{matrix}-\\0\end{matrix}\right] \\ &\quad \times \frac{1}{\Gamma(m_1)} \mathrm{G}_{1,2}^{1,1}\left[\frac{m_1\gamma}{\bar{\gamma}_1^{RF}}\middle|\begin{matrix}1\\m_1,0\end{matrix}\right]. \end{aligned} \tag{11}$$

III. Capacity Analysis

Based on the considered operation, we derive the ergodic capacity of the dual-hop hybrid FSO/RF system for the two system models. It was shown that the ergodic capacity can be used as an appropriate capacity metric for FSO/RF links by applying interleaving at the input of the link to ensure the FSO channel scintillation or the RF channel fading remains constant over one frame and varies for adjacent blocks. Also, by using a Gaussian codebook at the input of the channel. This codebook must be long enough for the scintillation/fading to reflect its ergodic nature (e.g., [23], [24]).

A. System Model I: With Single-Hop RF Backup Link

The ergodic capacity of the system under the single-hop RF backup link can be expressed as

$$\overline{C}^{(1)} = \overline{C}^{FSO}\left(\gamma_{th}^{FSO}\right) + P^{FSO}\left(\gamma_{th}^{FSO}\right) \cdot \overline{C}_{single}^{RF}\left(\gamma_{th}^{RF}\right), \tag{12}$$

where $P^{FSO}(\gamma_{th}^{FSO}) = F_{\gamma^{FSO}}(\gamma_{th}^{FSO})$. $\overline{C}^{FSO}(\gamma_{th}^{FSO})$ is the capacity of dual-hop FSO link, and $\overline{C}_{single}^{RF}(\gamma_{th}^{RF})$ represents the capacity of single-hop RF link, which are defined as

$$\begin{aligned} \overline{C}^{FSO}\left(\gamma_{th}^{FSO}\right) &= \int_{\gamma_{th}^{FSO}}^{\infty} W_{FSO} \cdot \log_2(1+\gamma)\, f_{\gamma^{FSO}}(\gamma) d\gamma \\ &= \frac{W_{FSO}}{\ln 2} \int_{\gamma_{th}^{FSO}}^{\infty} \mathrm{G}_{2,2}^{1,2}\left[\gamma\middle|\begin{matrix}1,1\\1,0\end{matrix}\right] f_{\gamma^{FSO}}(\gamma) d\gamma, \end{aligned} \tag{13}$$

and

$$\overline{C}_{single}^{RF}\left(\gamma_{th}^{RF}\right) = \frac{W_{RF}}{\ln 2} \int_{\gamma_{th}^{RF}}^{\infty} \mathrm{G}_{2,2}^{1,2}\left[\gamma\middle|\begin{matrix}1,1\\1,0\end{matrix}\right] f_{\gamma_{single}^{RF}}(\gamma) d\gamma, \tag{14}$$

where W_{FSO} and W_{RF} are the bandwidths of the high-priority FSO link and backup RF link, respectively. Using (6) in (13) results in

$$\begin{aligned} &\overline{C}^{FSO}\left(\gamma_{th}^{FSO}\right) \\ &= \frac{W_{FSO}}{\ln 2}\left(\int_{\gamma_{th}^{FSO}}^{\infty} \mathrm{G}_{2,2}^{1,2}\left[\gamma\middle|\begin{matrix}1,1\\1,0\end{matrix}\right] f_{\gamma_1^{FSO}}(\gamma) d\gamma\right. \\ &\quad + \int_{\gamma_{th}^{FSO}}^{\infty} \mathrm{G}_{2,2}^{1,2}\left[\gamma\middle|\begin{matrix}1,1\\1,0\end{matrix}\right] f_{\gamma_2^{FSO}}(\gamma) d\gamma \\ &\quad - \int_{\gamma_{th}^{FSO}}^{\infty} \mathrm{G}_{2,2}^{1,2}\left[\gamma\middle|\begin{matrix}1,1\\1,0\end{matrix}\right] f_{\gamma_1^{FSO}}(\gamma) F_{\gamma_2^{FSO}}(\gamma) d\gamma \\ &\quad \left. - \int_{\gamma_{th}^{FSO}}^{\infty} \mathrm{G}_{2,2}^{1,2}\left[\gamma\middle|\begin{matrix}1,1\\1,0\end{matrix}\right] F_{\gamma_1^{FSO}}(\gamma) f_{\gamma_2^{FSO}}(\gamma) d\gamma\right) \\ &= \frac{W_{FSO}}{\ln 2}\left(C_1^{FSO} + C_2^{FSO} - C_3^{FSO} - C_4^{FSO}\right). \end{aligned} \tag{15}$$

When the related PDF and CDF are substituted into (15), both C_1^{FSO} and C_2^{FSO} are solved using Appendix A, while C_3^{FSO} and C_4^{FSO} are solved using Appendix B, which can be written as

$$C_1^{FSO} = \frac{\phi_1^2}{2\Gamma(\alpha_1)\Gamma(\beta_1)}$$

$$\times \mathrm{H}_{1,1:2,2:1,3}^{1,0:1,2:3,0}\left[\gamma_{th}^{FSO}, \alpha_1\beta_1\xi_1\left(\frac{\gamma_{th}^{FSO}}{\bar{\gamma}_1}\right)^{\frac{1}{2}}\middle|\begin{matrix}(1;1,0.5)\\(0;1,0.5)\\(1;1),(1;1)\\(1;1),(0;1)\\\delta_1\\\delta_2\end{matrix}\right], \tag{16}$$

$$C_2^{FSO} = \frac{\phi_2^2}{2\Gamma(\alpha_2)\Gamma(\beta_2)}$$

$$\times \mathrm{H}_{1,1:2,2:1,3}^{1,0:1,2:3,0}\left[\gamma_{th}^{FSO}, \alpha_2\beta_2\xi_2\left(\frac{\gamma_{th}^{FSO}}{\bar{\gamma}_2}\right)^{\frac{1}{2}}\middle|\begin{matrix}(1;1,0.5)\\(0;1,0.5)\\(1;1),(1;1)\\(1;1),(0;1)\\\delta_3\\\delta_4\end{matrix}\right], \tag{17}$$

$$C_3^{FSO} = \frac{\phi_1^2\phi_2^2 2^{\alpha_2+\beta_2-4}}{\pi\Gamma(\alpha_1)\Gamma(\alpha_2)\Gamma(\beta_1)\Gamma(\beta_2)}\mathrm{H}_{1,1:2,2:3,7:1,3}^{1,0:1,2:6,1:3,0}$$

$$\left[\gamma_{th}^{FSO}, \left(\frac{\alpha_2\beta_2\xi_2}{4}\right)^2\frac{\gamma_{th}^{FSO}}{\bar{\gamma}_2}, \alpha_1\beta_1\xi_1\left(\frac{\gamma_{th}^{FSO}}{\bar{\gamma}_1}\right)^{\frac{1}{2}}\middle|\begin{matrix}(1;1,1,0.5)\\(0;1,1,0.5)\\(1;1),(1;1)\\(1;1),(0;1)\\\delta_5\\\delta_6\\\delta_1\\\delta_2\end{matrix}\right], \tag{18}$$

and

$$C_4^{FSO} = \frac{\phi_1^2\phi_2^2 2^{\alpha_1+\beta_1-4}}{\pi\Gamma(\alpha_1)\Gamma(\alpha_2)\Gamma(\beta_1)\Gamma(\beta_2)}\mathrm{H}_{1,1:2,2:3,7:1,3}^{1,0:1,2:6,1:3,0}$$

$$\left[\gamma_{th}^{FSO}, \left(\frac{\alpha_1\beta_1\xi_1}{4}\right)^2\frac{\gamma_{th}^{FSO}}{\bar{\gamma}_1}, \alpha_2\beta_2\xi_2\left(\frac{\gamma_{th}^{FSO}}{\bar{\gamma}_2}\right)^{\frac{1}{2}}\middle|\begin{matrix}(1;1,1,0.5)\\(0;1,1,0.5)\\(1;1),(1;1)\\(1;1),(0;1)\\\delta_7\\\delta_8\\\delta_3\\\delta_4\end{matrix}\right], \tag{19}$$

where $\delta_1 = (\phi_1^2+1;1)$, $\delta_2 = (\phi_1^2;1),(\alpha_1;1),(\beta_1;1)$, $\delta_3 = (\phi_2^2+1;1)$, $\delta_4 = (\phi_2^2;1),(\alpha_2;1),(\beta_2;1)$, $\delta_5 = (1;1),(\frac{\phi_2^2+1}{2};1)$, $(\frac{\phi_2^2+2}{2};1)$, $\delta_6 = (\frac{\phi_2^2}{2};1),(\frac{\phi_2^2+1}{2};1),(\frac{\alpha_2}{2};1),(\frac{\alpha_2+1}{2};1),(\frac{\beta_2}{2};1)$, $(\frac{\beta_2+1}{2};1),(0;1)$, $\delta_7 = (1;1),(\frac{\phi_1^2+1}{2};1),(\frac{\phi_1^2+2}{2};1)$, $\delta_8 = (\frac{\phi_1^2}{2};1)$, $(\frac{\phi_1^2+1}{2};1),(\frac{\alpha_1}{2};1),(\frac{\alpha_1+1}{2};1),(\frac{\beta_1}{2};1),(\frac{\beta_1+1}{2};1),(0;1)$ and $\mathrm{H}_{\cdot,\cdot:\cdot,\cdot:\cdot,\cdot}^{\cdot,\cdot:\cdot,\cdot:\cdot,\cdot}(\cdot,\cdot)$, and $\mathrm{H}_{\cdot,\cdot:\cdot,\cdot:\cdot,\cdot}^{\cdot,\cdot:\cdot,\cdot:\cdot,\cdot}(\cdot,\cdot,\cdot)$ are the bivariate and the trivariate Fox's H functions, respectively, which can be implemented using Python code provided in [25].

Substituting $f_{\gamma_{single}^{RF}}(\gamma)$ into (14), the capacity of the direct backup RF link can be rewritten as

$$\overline{C}_{single}^{RF}\left(\gamma_{th}^{RF}\right) = \frac{W_{RF}}{\ln 2}\left(\frac{m}{\bar{\gamma}^{RF}}\right)^m\frac{1}{\Gamma(m)} \times \int_{\gamma_{th}^{RF}}^{\infty}\gamma^{m-1}\,\mathrm{G}_{2,2}^{1,2}\left[\gamma\middle|\begin{matrix}1,1\\1,0\end{matrix}\right]\mathrm{G}_{0,1}^{1,0}\left[\frac{m\gamma}{\bar{\gamma}^{RF}}\middle|\begin{matrix}-\\0\end{matrix}\right]d\gamma. \tag{20}$$

Utilizing Appendix A, yields

$$\overline{C}_{single}^{RF}\left(\gamma_{th}^{RF}\right) = \frac{W_{RF}}{\ln 2}\left(\frac{m}{\bar{\gamma}^{RF}}\right)^m\frac{\left(\gamma_{th}^{RF}\right)^m}{\Gamma(m)} \times \mathrm{H}_{1,1:2,2:0,1}^{1,0:1,2:1,0}\left[\gamma_{th}^{RF}, \frac{m}{\bar{\gamma}^{RF}}\gamma_{th}^{RF}\middle|\begin{matrix}(1-m;1,1)\\(-m;1,1)\\(1;1),(1;1)\\(1;1),(0;1)\\-\\(0;1)\end{matrix}\right]. \tag{21}$$

B. System Model II: With Dual-Hop RF Backup Link

In this scenario, the ergodic capacity of the system can be defined as

$$\overline{C}^{(2)} = \overline{C}^{FSO}\left(\gamma_{th}^{FSO}\right) + P^{FSO}\left(\gamma_{th}^{FSO}\right)\cdot\overline{C}_{dual}^{RF}\left(\gamma_{th}^{RF}\right), \tag{22}$$

where $\overline{C}^{FSO}(\gamma_{th}^{FSO})$ is given in (15). $\overline{C}_{dual}^{RF}(\gamma_{th}^{RF})$ is the capacity of dual-hop backup RF link which is defined as

$$\overline{C}_{dual}^{RF}\left(\gamma_{th}^{RF}\right) = \frac{W_{RF}}{2\ln 2}\int_{\gamma_{th}^{RF}}^{\infty}\mathrm{G}_{2,2}^{1,2}\left[\gamma\middle|\begin{matrix}1,1\\1,0\end{matrix}\right]f_{\gamma_{dual}^{RF}}(\gamma)\,d\gamma. \tag{23}$$

Using (11) in (23), we get

$$\begin{aligned}\overline{C}_{dual}^{RF}\left(\gamma_{th}^{RF}\right) &= \frac{W_{RF}}{2\ln 2}\\ &\left(\int_{\gamma_{th}^{RF}}^{\infty}\mathrm{G}_{2,2}^{1,2}\left[\gamma\middle|\begin{matrix}1,1\\1,0\end{matrix}\right]f_{\gamma_1^{RF}}(\gamma)\,d\gamma\right.\\ &+\int_{\gamma_{th}^{RF}}^{\infty}\mathrm{G}_{2,2}^{1,2}\left[\gamma\middle|\begin{matrix}1,1\\1,0\end{matrix}\right]f_{\gamma_2^{RF}}(\gamma)\,d\gamma\\ &-\int_{\gamma_{th}^{RF}}^{\infty}\mathrm{G}_{2,2}^{1,2}\left[\gamma\middle|\begin{matrix}1,1\\1,0\end{matrix}\right]f_{\gamma_1^{RF}}(\gamma)\,F_{\gamma_2^{RF}}(\gamma)\,d\gamma\\ &\left.-\int_{\gamma_{th}^{RF}}^{\infty}\mathrm{G}_{2,2}^{1,2}\left[\gamma\middle|\begin{matrix}1,1\\1,0\end{matrix}\right]F_{\gamma_1^{RF}}(\gamma)\,f_{\gamma_2^{RF}}(\gamma)\,d\gamma\right)\\ &= \frac{W_{RF}}{2\ln 2}\left(C_1^{RF}+C_2^{RF}-C_3^{RF}-C_4^{RF}\right)\end{aligned} \tag{24}$$

Through the substitution of the related PDF and CDF into (24), both C_1^{RF} and C_2^{RF} can be solved using Appendix A, whereas C_3^{RF} and C_4^{RF} are solved using Appendix B. After some manipulation, the following aligns result:

$$C_1^{RF} = \left(\frac{m_1}{\bar{\gamma}_1^{RF}}\right)^{m_1}\frac{\left(\gamma_{th}^{RF}\right)^{m_1}}{\Gamma(m_1)}$$

$$\times \mathrm{H}^{1,0:1,2:1,0}_{1,1:2,2:0,1}\left[\gamma_{th}^{RF}, \frac{m_1}{\bar{\gamma}_1^{RF}}\gamma_{th}^{RF} \middle| \begin{matrix}(1-m_1;1,1)\\(-m_1;1,1)\\(1;1),(1;1)\\(1;1),(0;1)\\-\\(0;1)\end{matrix}\right], \tag{25}$$

$$C_2^{RF} = \left(\frac{m_2}{\bar{\gamma}_2^{RF}}\right)^{m_2} \frac{\left(\gamma_{th}^{RF}\right)^{m_2}}{\Gamma(m_2)} \times \mathrm{H}^{1,0:1,2:1,0}_{1,1:2,2:0,1}\left[\gamma_{th}^{RF}, \frac{m_2}{\bar{\gamma}_2^{RF}}\gamma_{th}^{RF} \middle| \begin{matrix}(1-m_2;1,1)\\(-m_2;1,1)\\(1;1),(1;1)\\(1;1),(0;1)\\-\\(0;1)\end{matrix}\right], \tag{26}$$

$$C_3^{RF} = \left(\frac{m_1}{\bar{\gamma}_1^{RF}}\right)^{m_1} \frac{\left(\gamma_{th}^{RF}\right)^{m_1}}{\Gamma(m_1)\Gamma(m_2)} \mathrm{H}^{1,0:1,2:1,0:1,1}_{1,1:2,2:0,1:1,2} \left[\gamma_{th}^{RF}, \frac{m_1}{\bar{\gamma}_1^{RF}}\gamma_{th}^{RF}, \frac{m_2}{\bar{\gamma}_2^{RF}}\gamma_{th}^{RF} \middle| \begin{matrix}(1-m_1;1,1)\\(-m_1;1,1)\\(1;1),(1;1)\\(1;1),(0;1)\\-\\(0;1)\\(1;1)\\(m_2;1),(0;1)\end{matrix}\right], \tag{27}$$

and

$$C_4^{RF} = \left(\frac{m_2}{\bar{\gamma}_2^{RF}}\right)^{m_2} \frac{\left(\gamma_{th}^{RF}\right)^{m_2}}{\Gamma(m_1)\Gamma(m_2)} \mathrm{H}^{1,0:1,2:1,0:1,1}_{1,1:2,2:0,1:1,2} \left[\gamma_{th}^{RF}, \frac{m_2}{\bar{\gamma}_2^{RF}}\gamma_{th}^{RF}, \frac{m_1}{\bar{\gamma}_1^{RF}}\gamma_{th}^{RF} \middle| \begin{matrix}(1-m_2;1,1)\\(-m_2;1,1)\\(1;1),(1;1)\\(1;1),(0;1)\\-\\(0;1)\\(1;1)\\(m_1;1),(0;1)\end{matrix}\right]. \tag{28}$$

IV. Numerical and Simulation Results

In this section, we present numerical results for the ergodic capacity of the two considered systems derived in Section III. Additionally, we provide Monte Carlo simulations for validation, where we generate 10^6 samples of the random variable (RV). The FSO fading channel is represented by the product of two Gamma RVs, whereas the pointing error is represented by the Rayleigh RV. To calculate the expressions in terms of bivariate and trivariate Fox's H functions, we used the code in [25]. Without loss of generality, the transmitted power per hop for the FSO link is assumed to be equal (i.e., $P_{FSO,1} = P_{FSO,2} = P_{FSO}/2$), also to ensure fairness in comparing the two RF setups, we assume equal end-to-end RF transmitted power (i.e., $P_{RF,1} = P_{RF,2} = P_{RF}/2$) for the dual-hop RF link, and P_{RF} for the direct RF link. Furthermore, the turbulence and pointing errors parameters are also assumed to be equal (i.e. $\alpha_1 = \alpha_2$, $\beta_1 = \beta_2$, $\phi_1 = \phi_2$), and the fading parameter of Nakagami-m fading $m_1 = m_2 = m = 2$. Moderate and strong turbulence are characterized by $C_n^2 = 3 \times 10^{-14}\,\mathrm{m}^{-\frac{2}{3}}$, and $C_n^2 = 1 \times 10^{-13}\,\mathrm{m}^{-\frac{2}{3}}$, respectively. Other parameters are set as follows: wavelength $\lambda = 1550$ nm, $\eta = 0.5$, $\theta = 1$ mrad, $\sigma = 0.43$, $R_o = 10$ cm, $\gamma_{th}^{FSO} = \gamma_{th}^{RF} = 5$ dB, and hop's distance $L_1 = L_2 = L/2$ for dual-hop, where $L = 2$ km is the total distance, except for Fig. 4. The rest simulation parameters can be found in [2].

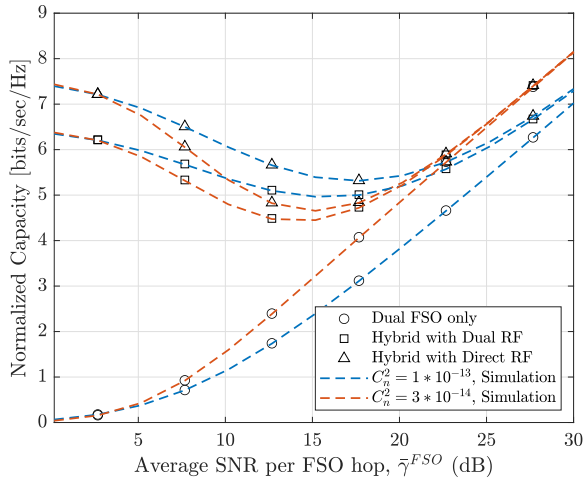

Fig. 1. Ergodic capacity of the system in both scenarios under strong and moderate turbulence with $\phi = 3.354$, and $P_{RF} = 15$ dBm.

In Fig. 1, the ergodic capacity of the system in both scenarios, given in (12) and (22), is presented under different turbulence conditions with pointing error ($\phi = 3.354$), and for the case when the backup RF link has good quality ($P_{RF} = 15$ dBm). It can be shown that the capacity decreases as the strength of the turbulence conditions increases in cases where the FSO link dominates the transmission. For instance, at $\bar{\gamma}^{FSO} = 25$ dB, for the hybrid system with dual-hop RF link scenario, the capacity under strong turbulence conditions is reduced by almost 8% compared to the capacity under moderate turbulence conditions. In addition, one can notice that the capacity performance is improved in both scenarios compared to that of dual-hop FSO-only. In more detail, at lower values of $\bar{\gamma}^{FSO}$, the system switches frequently to the high-quality RF link, and as the value of $\bar{\gamma}^{FSO}$ increases, the system relies more on the FSO link where its capacity starts to converge to that of the dual-hop FSO-only system.

Fig. 2 shows the impact of the pointing errors ϕ on the ergodic capacity of the system in both scenarios under strong turbulence conditions with $P_{RF} = 10$ dBm. It can be observed that for both the hybrid and dual-hop FSO-only systems, the capacity performance decreases as the strength of the pointing error increases (i.e., the value of ϕ becomes smaller) at higher values of $\bar{\gamma}^{FSO}$. Furthermore, one can notice that the capacity performance of the hybrid system with direct RF link scenario

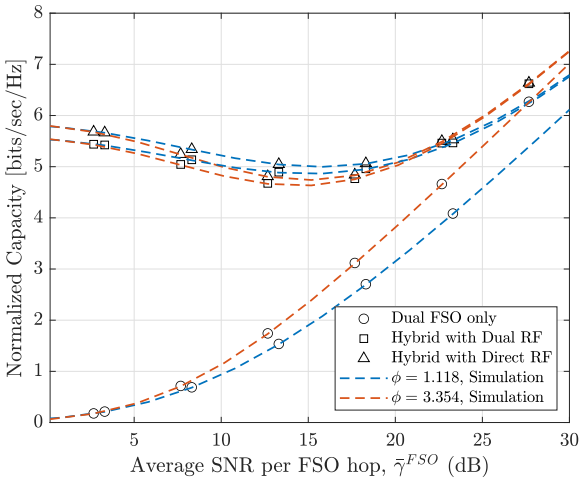

Fig. 2. Ergodic Capacity of the system in both scenarios under strong turbulence with $P_{RF} = 10$ dBm, and various values of ϕ.

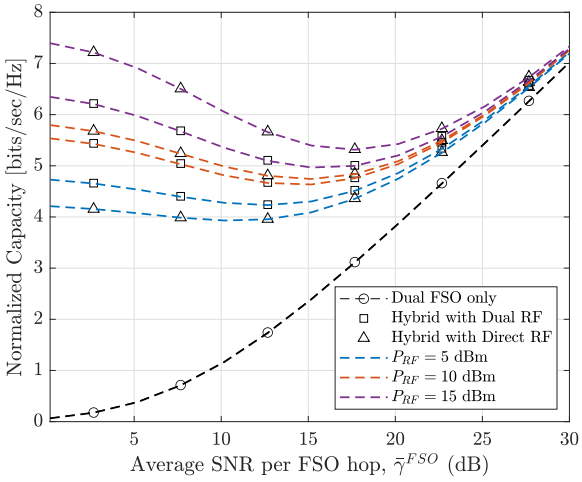

Fig. 3. Ergodic Capacity of the system in both scenarios under strong turbulence with $\phi = 3.354$, and different values of P_{RF}.

is better than that of the hybrid system with dual-hop RF link scenario especially under good RF link conditions.

The effects of varying P_{RF} and the total distance on the ergodic capacity of the system are presented in Figs. 3 and 4, respectively. In Fig. 3, the total distance is kept fixed, and P_{RF} is varied, while in Fig. 4, P_{RF} is fixed, and the total distance is varied. This allows us to investigate their effects separately. It can be observed that low P_{RF} is insufficient to counteract the effect of channel fading in the direct link scenario. However, in the dual-hop link scenario, where the distance of each hop is half of the total link distance, the effect of channel fading is reduced, resulting in a better system capacity. As P_{RF} increases, the received average SNR improves in both scenarios. However, due to the half-duplex assumption, the capacity in the direct link scenario becomes better than that in the dual-hop link scenario.

In Fig. 4, we examine the effect of varying the total distance, while keeping P_{RF} at a good level for both links ($P_{RF} =$ 13 dBm). It can be observed that initially the FSO link dominates

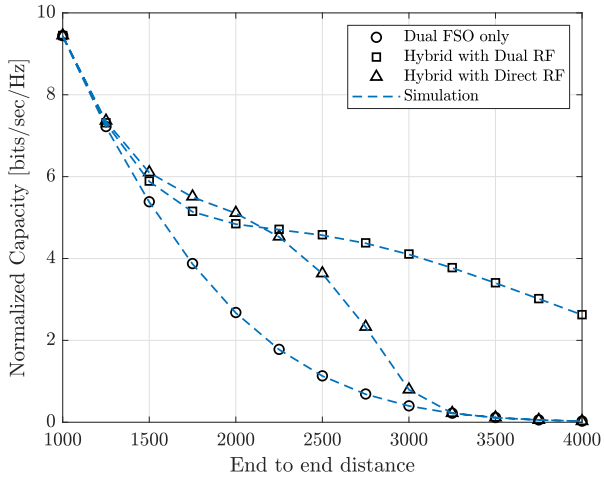

Fig. 4. Ergodic Capacity of the system in both scenarios under strong turbulence with $\phi = 3.354$, and $P_{FSO} = 13$ dBm.

the transmission. However, as the distance increases, the system relies more on the backup link, and the capacity of the direct link scenario is slightly higher than that of the dual-hop link scenario due to the half-duplex assumption. At larger distances, the dual-hop link scenario offers a superior capacity gain over the direct link scenario. Finally, the simulation results match well with the analytical results.

V. Conclusion

In this work, the ergodic capacity performances of two hybrid FSO/RF systems with DF relaying were investigated under the effect of strong atmospheric turbulence and pointing errors. A single-hop RF backup link was considered in the first system, and a dual-hop RF backup link was considered in the second system. The FSO link is modeled by the gamma-gamma fading channel, and the RF link is modeled by the Nakagami-m fading channel. The CDFs and PDFs for both systems were obtained to be used for derivation of the exact expressions of the ergodic capacity. The results showed the effects of various turbulence conditions as well as the effects of pointing errors. Also, the results indicated the amount of gain that the two considered systems are able to provide when compared to the conventional dual-hop FSO system.

Appendix A

$$I_1 = \int_{x_o}^{\infty} x^{v-1} \mathrm{G}_{p,q}^{m,n}\left[\alpha x \,\middle|\, \begin{matrix} a_1,\ldots,a_p \\ b_1,\ldots,b_q \end{matrix}\right] \times \mathrm{G}_{p_1,q_1}^{m_1,n_1}\left[\beta x^{\rho} \,\middle|\, \begin{matrix} a_{11},\ldots,a_{1p_1} \\ b_{11},\ldots,b_{1q_1} \end{matrix}\right] dx. \tag{29}$$

Initially, we start with the change of variable $x = x_o\, y$, $x_1 = 1/(\alpha x_o)$, and $x_2 = 1/(x_o \beta^{1/\rho})$. Then

$$I_1 = x_o^v \int_0^{\infty} y^{v-1} u\,(y-1)\, \mathrm{G}_{p,q}^{m,n}\left[\frac{y}{x_1} \,\middle|\, \begin{matrix} a_1,\ldots,a_p \\ b_1,\ldots,b_q \end{matrix}\right]$$

$$\times \mathrm{G}_{p_1,q_1}^{m_1,n_1}\left[\left(\frac{y}{x_2}\right)^{\rho}\middle|\begin{matrix}a_{11},\ldots,a_{1p_1}\\ b_{11},\ldots,b_{1q_1}\end{matrix}\right]dy$$

$$= x_o^v\int_0^{\infty}\frac{1}{y}g_o(y)g_1\left(\frac{y}{x_1}\right)g_2\left(\left(\frac{y}{x_2}\right)^{\rho}\right)dy, \tag{30}$$

where, $g_o(y) = y^v u(y-1)$, and $u(.)$ is a unit step function, $g_1\left(\frac{y}{x_1}\right) = \mathrm{G}_{p,q}^{m,n}\left[\frac{y}{x_1}\middle|\begin{matrix}a_1,\ldots,a_p\\ b_1,\ldots,b_q\end{matrix}\right]$, and $g_2\left(\left(\frac{y}{x_2}\right)^{\rho}\right) = \mathrm{G}_{p_1,q_1}^{m_1,n_1}\left[\left(\frac{y}{x_2}\right)^{\rho}\middle|\begin{matrix}a_{11},\ldots,a_{1p_1}\\ b_{11},\ldots,b_{1q_1}\end{matrix}\right]$. (30) can be solved using Mellin convolution theorem and Mellin transform technique [26]. The Mellin transform of $g_o(y)$, $g_1(y)$, and $g_2(y^{\rho})$ are given as [27]

$$G_o(s) = \frac{\Gamma(-s-v)}{\Gamma(1-s-v)}$$

$$G_1(s) = \frac{\prod_{j=1}^{m}\Gamma(b_j+s)\prod_{j=1}^{n}\Gamma(1-a_j-s)}{\prod_{j=m+1}^{q}\Gamma(1-b_j-s)\prod_{j=n+1}^{p}\Gamma(a_j+s)}$$

$$G_2(s) = \frac{1}{|\rho|}\frac{\prod_{j=1}^{m_1}\Gamma(b_{1j}+s/\rho)\prod_{j=1}^{n_1}\Gamma(1-a_{1j}-s/\rho)}{\prod_{j=m_1+1}^{q_1}\Gamma(1-b_{1j}-s/\rho)\prod_{j=n_1+1}^{p_1}\Gamma(a_{1j}+s/\rho)}. \tag{31}$$

Then (30) can be rewritten as

$$I_1 = \frac{{x_o}^v}{(2\pi i)^2}\int_{R_1}\int_{R_2}\rho G_o(s_1+\rho s_2)G_1(-s_1)G_2(-\rho s_2)$$
$$\times x_1^{-s_1}x_2^{-\rho s_2}ds_1ds_2. \tag{32}$$

Using the definition of H-function of two variables in [28, (2.56)], I_1 can be solved as

$$I_1 = x_o^v\mathrm{H}_{1,1:p,q:p_1,q_1}^{1,0:m,n:m_1,n_1}\left[\alpha x_o,\beta x_o^{\rho}\middle|\begin{matrix}(1-v;1,\rho)\\ (-v;1,\rho)\\ (a_j;1)_{1,p}\\ (b_j;1)_{1,q}\\ (a_{1j};1)_{1,p_1}\\ (b_{1j};1)_{1,q_1}\end{matrix}\right]. \tag{33}$$

Appendix B

$$I_2 = \int_{x_o}^{\infty}x^{v-1}\mathrm{G}_{p,q}^{m,n}\left[\alpha x\middle|\begin{matrix}a_1,\ldots,a_p\\ b_1,\ldots,b_q\end{matrix}\right]$$
$$\times\mathrm{G}_{p_1,q_1}^{m_1,n_1}\left[\beta x\middle|\begin{matrix}a_{11},\ldots,a_{1p_1}\\ b_{11},\ldots,b_{1q_1}\end{matrix}\right]\mathrm{G}_{p_2,q_2}^{m_2,n_2}\left[\tau x^{\rho}\middle|\begin{matrix}a_{21},\ldots,a_{2p_2}\\ b_{21},\ldots,b_{2q_2}\end{matrix}\right]dx. \tag{34}$$

Let $x = x_o\,y$, $x_1 = 1/(\alpha x_o)$, $x_2 = 1/(x_o\beta^{1/\rho})$, and $x_3 = 1/(x_o\tau^{1/\rho})$. Then

$$I_2 = x_o^v\int_0^{\infty}y^{v-1}u(y-1)\,\mathrm{G}_{p,q}^{m,n}\left[\frac{y}{x_1}\middle|\begin{matrix}a_1,\ldots,a_p\\ b_1,\ldots,b_q\end{matrix}\right]$$
$$\times\mathrm{G}_{p_1,q_1}^{m_1,n_1}\left[\frac{y}{x_2}\middle|\begin{matrix}a_{11},\ldots,a_{1p_1}\\ b_{11},\ldots,b_{1q_1}\end{matrix}\right]\mathrm{G}_{p_2,q_2}^{m_2,n_2}\left[\left(\frac{y}{x_3}\right)^{\rho}\middle|\begin{matrix}a_{21},\ldots,a_{2p_2}\\ b_{21},\ldots,b_{2q_2}\end{matrix}\right]dy$$
$$= x_o^v\int_0^{\infty}\frac{1}{y}f_{\circ}(y)f_1\left(\frac{y}{x_1}\right)f_2\left(\frac{y}{x_2}\right)f_3\left(\frac{y}{x_3}\right)dy. \tag{35}$$

Notice that $f_o(y)$ has the same form as $g_o(y)$, $f_1(y)$ and $f_2(y)$ have the same form as $g_1(y)$, and $f_3(y^{\rho})$ has similar form as $g_2(y^{\rho})$. Therefore, The Mellin transforms $F_o(s)$, $F_1(s)$, $F_2(s)$, and $F_3(s)$ are found using (31). Then, (35) can be rewritten as

$$I_1 = \frac{{x_o}^v}{(2\pi i)^2}\int_{R_1}\int_{R_2}\int_{R_3}\rho F_o(s_1+s_2+\rho s_3)F_1(-s_1)F_2(-s_2)$$
$$\times F_3(-\rho s_3)x_1^{-s_1}x_2^{-s_2}x_3^{-\rho s_3}ds_1ds_2ds_3. \tag{36}$$

With the help of [28, (A.1], I_2 can be solved as

$$I_2 = x_o^v\mathrm{H}_{1,1:p,q:p_1,q_1}^{1,0:m,n:m_1,n_1:m_2,n_2}\left[vx_o,\beta x_o,\tau x_o^{\rho}\middle|\begin{matrix}(1-v;1,\rho)\\ (-v;1,\rho)\\ (a_j;1)_{1,p}\\ (b_j;1)_{1,q}\\ (a_{1j};1)_{1,p_1}\\ (b_{1j};1)_{1,q_1}\\ (a_{2j};1)_{1,p_2}\\ (b_{2j};1)_{1,q_2}\end{matrix}\right]. \tag{37}$$

References

[1] Z. Ghassemlooy and W. O. Popoola, "Terrestrial free-space optical communications," in *Mobile and Wireless Communications Network Layer and Circuit Level Design*. London, U.K.: InTech, 2010, pp. 355–391.

[2] W. A. Alathwary and E. S. Altubaishi, "On the performance analysis of decode-and-forward multi-hop hybrid FSO/RF systems with hard-switching configuration," *IEEE Photon. J.*, vol. 11, no. 6, Dec. 2019, Art. no. 7907012.

[3] M. Aggarwal, P. Garg, and P. Puri, "Dual-hop optical wireless relaying over turbulence channels with pointing error impairments," *J. Lightw. Technol.*, vol. 32, no. 9, pp. 1821–1828, May 2014.

[4] S. Anees and M. R. Bhatnagar, "On the capacity of decode-and-forward dual-hop free space optical communication systems," in *Proc. IEEE Wireless Commun. Netw. Conf.*, 2014, pp. 18–23.

[5] J. Zhang, L. Dai, Y. Zhang, and Z. Wang, "Unified performance analysis of mixed radio frequency/free-space optical dual-hop transmission systems," *J. Lightw. Technol.*, vol. 33, no. 11, pp. 2286–2293, Jun. 2015.

[6] E. Balti and M. Guizani, "Mixed RF/FSO cooperative relaying systems with co-channel interference," *IEEE Trans. Commun.*, vol. 66, no. 9, pp. 4014–4027, Sep. 2018.

[7] L. Chen and W. Wang, "Multi-diversity combining and selection for relay-assisted mixed RF/FSO system," *Opt. Commun.*, vol. 405, pp. 1–7, 2017.

[8] B. Bag, A. Das, A. Chandra, and C. Bose, "Capacity analysis for Rayleigh/gamma-gamma mixed RF/FSO link with fixed-gain AF relay," *IEICE Trans. Commun.*, vol. 100, no. 10, pp. 1747–1757, 2017.

[9] J. Vellakudiyan, V. Palliyembil, I. S. Ansari, P. Muthuchidambaranathan, and K. A. Qaraqe, "Performance analysis of the decode-and-forward relay-based RF-FSO communication system in the presence of pointing errors," *IET Signal Process.*, vol. 13, no. 4, pp. 480–485, 2019.

[10] B. Ashrafzadeh, E. Soleimani-Nasab, M. Kamandar, and M. Uysal, "A framework on the performance analysis of dual-hop mixed FSO-RF cooperative systems," *IEEE Trans. Commun.*, vol. 67, no. 7, pp. 4939–4954, Jul. 2019.

[11] Q. Sun, Z. Zhang, Y. Zhang, M. Lopez-Benitez, and J. Zhang, "Performance analysis of dual-hop wireless systems over mixed FSO/RF fading channel," *IEEE Access*, vol. 9, pp. 85529–85542, 2021.

[12] T. Rakia, H.-C. Yang, M.-S. Alouini, and F. Gebali, "Outage analysis of practical FSO/RF hybrid system with adaptive combining," *IEEE Commun. Lett.*, vol. 19, no. 8, pp. 1366–1369, Aug. 2015.

[13] A. Touati, A. Abdaoui, F. Touati, M. Uysal, and A. Bouallegue, "On the effects of combined atmospheric fading and misalignment on the hybrid FSO/RF transmission," *J. Opt. Commun. Netw.*, vol. 8, no. 10, pp. 715–725, 2016.

[14] M. Siddharth, S. Shah, N. Vishwakarma, and R. Swaminathan, "Performance analysis of adaptive combining based hybrid FSO/RF terrestrial communication," *IET Commun.*, vol. 14, no. 22, pp. 4057–4068, 2020.

[15] L. Huang et al., "Unified performance analysis of hybrid FSO/RF system with diversity combining," *J. Lightw. Technol.*, vol. 38, no. 24, pp. 6788–6800, Dec. 2020.

[16] Y. Wu, M. Jiang, G. Li, and D. Kong, "Systematic performance analysis of hybrid FSO/RF system over generalized fading channels with pointing errors," *Photonics*, vol. 9, no. 11, Nov. 2022, Art. no. 873.

[17] S. Sharma, A. Madhukumar, and R. Swaminathan, "Switching-based cooperative decode-and-forward relaying for hybrid FSO/RF networks," *J. Opt. Commun. Netw.*, vol. 11, no. 6, pp. 267–281, 2019.

[18] K. A. Alhamawi and E. S. Altubaishi, "Performance analysis of an AF dual-hop FSO communication system with RF backup link," *Curr. Opt. Photon.*, vol. 3, no. 4, pp. 311–319, 2019.

[19] S. Sharma, A. Madhukumar, and S. Ramabadran, "Performance optimisation for dual-hop hybrid FSO/RF system with selection combining," *IET Optoelectron.*, vol. 14, no. 6, pp. 422–433, 2020.

[20] N. D. Chatzidiamantis, G. K. Karagiannidis, E. E. Kriezis, and M. Matthaiou, "Diversity combining in hybrid RF/FSO systems with PSK modulation," in *Proc. IEEE Int. Conf. Commun.*, 2011, pp. 1–6.

[21] "Meijer G-function: Integration (formula 07.34.21.0084)." [Online]. Available: https://functions.wolfram.com/07.34.21.0084.01

[22] E. S. Altubaishi, "On the performance of all-optical amplify-and-forward relaying with a backup radio-frequency link over strong atmospheric turbulence and misalignment fading," *Curr. Opt. Photon.*, vol. 5, no. 2, pp. 114–120, 2021.

[23] M. I. Petkovic, I. S. Ansari, G. T. Djordjevic, and K. A. Qaraqe, "Error rate and ergodic capacity of RF-FSO system with partial relay selection in the presence of pointing errors," *Opt. Commun.*, vol. 438, pp. 118–125, 2019.

[24] M. Z. Hassan, M. J. Hossain, and J. Cheng, "Ergodic capacity comparison of optical wireless communications using adaptive transmissions," *Opt. Exp.*, vol. 21, no. 17, pp. 20346–20362, 2013.

[25] H. R. Alhennawi, M. M. H. El Ayadi, M. H. Ismail, and H.-A. M. Mourad, "Closed-form exact and asymptotic expressions for the symbol error rate and capacity of the H-function fading channel," *IEEE Trans. Veh. Technol.*, vol. 65, no. 4, pp. 1957–1974, Apr. 2016.

[26] "General mathematical identities for analytic functions: Integral transforms." [Online]. Available: https://functions.wolfram.com/GeneralIdentities/11/

[27] A. Erdilyi, W. Magnus, F. Oberhettinger, and F. Tricomi, *Tables of integral transforms*, vol. I, New York, NY, USA: McGraw-Hill, 1954.

[28] A. M. Mathai, R. K. Saxena, and H. J. Haubold, *The H-Function: Theory and Applications*. Berlin, Germany: Springer, 2009.